Ir(III) complexes designed for light-emitting devices: beyond the luminescence color array

Kassio Papi Silva Zanoni, Rodolfo Lopes Coppo, Ronaldo Costa Amaral, Neyde Yukie Murakami Iha

Laboratory of Photochemistry and Energy Conversion, Departamento de Química Fundamental, Instituto de Química, Universidade de São Paulo - USP, Av. Prof. Lineu Prestes, 748, 05508-000 São Paulo, SP, Brazil.

ABSTRACT

In pursuing novel efficient lightning technologies and materials, phosphorescent cyclometallated Ir(III) complexes have been prominent due to their wide color arrays and highly efficient electroluminescence. Their photophysical properties are strongly influenced by spin-orbit coupling exerted by the iridium core, usually resulting in intense, short-lived emission, which can be systematically tuned as a triumph of the molecular engineering. This *Perspective* aims to present recent breakthroughs and state of the art on emissive Ir(III) compounds, in particular a personal account on heteroleptic $[Ir(N^C)_2(L^X)]^+$ complexes, addressing the mechanistic concepts behind their luminescence. Their fascinating photophysical properties strengthen application in more-efficient light-emitting technologies, such as organic light-emitting diodes and light-emitting electrochemical cells.
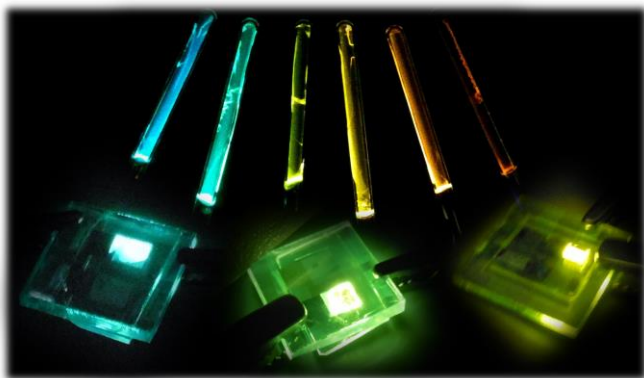
TABLE OF CONTENTS ENTRY

TABLE OF CONTENTS SYNOPSIS

This *Perspective* highlights photophysics and recent breakthroughs on emissive Ir(III) compounds, including a personal account elucidating the role of molecular and electronic structure in controlling the photophysics of heteroleptic $[Ir(N^{\wedge}C)_2(L^{\wedge}X)]^+$ complexes.

INTRODUCTION

Light-emitting devices (LEDs) have emerged as alternative to conventional incandescent and fluorescent lamps because of their efficient light generation, resulting in low power consumption, low voltage and low current operation, fast response time, long durability, high performance and low maintenance, due to eco-friendly fabrication processes.[1–4] Organic light-emitting devices (OLEDs)[5–8] and light-emitting electrochemical cells (LECs)[9–12] find applications in computers, mobile phones, TV sets, watches and displays, as low-energy-consumption devices.[4–6,8,13]

Research on OLEDs and LECs mainly focus on multi-color, highly-emissive complexes and new techniques for device fabrication. For this purpose, iridium(III) coordination compounds have played a prominent role in many application in photonics, as biological phosphorescent labels and sensors,[14–18] photodynamic therapy,[15,17] metallopharmaceuticals with antitumoral activities,[17] dye-sensitized solar cells,[19–22] and catalysis.[23–27] Most investigations have focused on photophysical properties, with promising applications in the active luminescent layers of OLEDs and LECs.[7,8,28] The choice of Ir(III) is keyed to its high spin-orbit coupling (SOC), $\xi_{Ir} = 4430 \text{ cm}^{-1}$,[29] and on the very strong electronic interaction between the metal-core and ligands through the metal-ligand bonds.[30] These characteristics lead to remarkable and unique features, including excellent thermal and photochemical stabilities with a variety of ligands, relatively short-lived excited states, impressive emission quantum yields and color variety through judicious molecular engineering by control of ligands.[29–40]

In this *Perspective*, we report recent breakthroughs and the state of the art on highly-efficient emissive Ir(III) complexes including a personal account elucidating the role of

molecular and electronic structure in controlling the photophysics of heteroleptic Ir(III) compounds of importance in light-emitting devices.[28,29,40,41]

PHOTOPHYSICS OF Ir(III) COMPLEXES

Principles

Emissive decay from excited to ground states occurs through a combination of radiative (k_r) and non-radiative processes (k_{nr}), with their corresponding rate constants related to the excited-state lifetime (τ) and the emission quantum yield (ϕ) as shown in Equations 1 and 2.[42–44]

$$\phi = \frac{k_r}{k_r + k_{nr}} \tag{1}$$

$$\tau = \frac{1}{k_r + k_{nr}} \tag{2}$$

Emission is usually due to a phosphorescence from a formally spin-forbidden $T_1 \rightarrow S_0$ transition which is facilitated by the high spin orbit coupling (SOC) constant for Ir(III) of $\sim 4 \times 10^3$ cm^{-1}.[8,45] The high magnitude SOC constants for the 5d elements – notably for iridium, osmium and platinum – plays a very important role in their excited-state decay.[29,45] In addition, charge transfer (CT) transitions tend to have higher phosphorescent yields with higher k_r values because of their higher transition dipole moments,[8,29,34,44] as will be discussed below. Phosphorescence from ligand centered (LC) excited states exhibit similar τ and spectral shape to the free ligand emission. Metal centered *d-d* transitions are the least emissive ($\phi \sim 10^{-5}$)[5] and typically undergo rapid, non radiative decay, often accompanied by ligand loss.

Since 2000, the synthesis of novel Ir(III) phosphorescent complexes has received new emphasis due to their strong phosphorescence from MLCT triplet states that have led to both applications and strategic understanding for LED fabrication with the importance of high emission yields and microsecond lifetimes.[5,13] Another desired characteristic is their high photo and thermal stabilities, which enable long device lifetime. Adjusting ligands allows for emitting complexes in all three of the primary color – blue, green and red – as featured in the following sections.

Heteroleptic Ir(III) Complexes

The three bidentate ligands coordinated to the Ir(III) with neutral nitrogen or monoanionic carbon/oxygen/sulfur atoms, Figure 1, give highly phosphorescent Ir(III) compounds. Two of the ligands are identical, organometallated to Ir(III) through *N^C* atoms in a 5-membered metallacycle, with a very-strong quasi-covalent bond between Ir(III) and carbon. These *N^C* ligands are often named cyclometallated or attached, being 2-phenylpyridine (*ppy*) a typical example and derivatives. The third bidentate ligand can be the same *N^C* ligand (homoleptic) or a different ligand or ligands (heteroleptic), in which case the ancillary ligand is abbreviated as *L^X*.
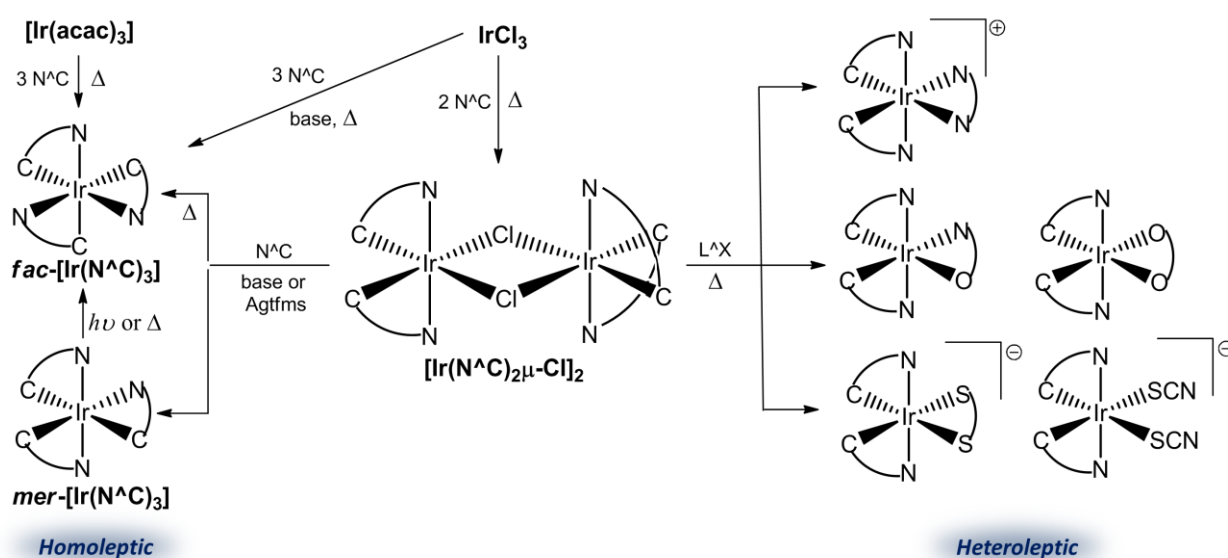
Figure 1. Molecular structures and synthetic routes for different types of Ir(III) complexes.

Heteroleptic complexes are usually synthesized from the μ-dichloro-bridged precursor [Ir(*N^C*)$_2$μ-Cl]$_2$[46] and an ancillary *L^X* ligand; the *N^C* ligands in heteroleptic products are in a *trans*-N,N configuration.[47] The ancillary ligand can be neutral or negatively-charged playing an important role in determining the charge of the heteroleptic complex. Diimine *N^N* ligands, such as bipyridine, phenantroline and pyridiltriazoles, lead to cationic complexes,[29] while picolinates *N^O*[40,48] or acetylacetonates *O^O*[49,50] lead to neutral compounds. Anionic Ir(III) complexes are not very common and few reported compounds contain cyanides and

thiocyanates[51] or dithiolates and sulfinates[52] as *L^X* ligands. Recently, the use of an orotate *N^O* ancillary ligand led to an anionic complex with quasi-covalent bonds for both Ir–O and Ir–N.[53]

Coordination of a third cyclometallated *N^C* ligand leads to a homoleptic complex with a thermodynamically favored facial-configuration (*fac-*). The *fac*-isomers are obtained by refluxing either [Ir(*acac*)$_3$] (*acac* = acetylacetonate) with three equivalents of *N^C*[54] or [(Ir(*N^C*)$_2\mu$-Cl$_2$]$_2$ in the presence of base or silver triflate (Agtfms).[55] The kinetically favored meridional-complex (*mer-*) is obtained with careful control of the synthetic condition and the reaction temperature. The *mer-* isomers can be converted to the *fac*-isomers by thermal or photochemical conversion.[56–58]
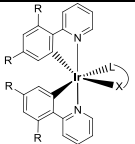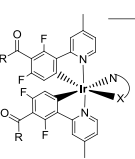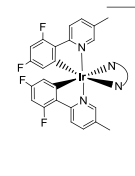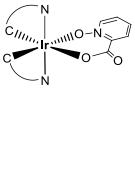
The many options for ligands and conformations lead to variations in electronic properties that, by ligand tuning, can be used to influence the pathways that dominate excitation and deactivation.[32,59,60] Understanding of the nature of ground and excited states and their interactions is crucial in exploiting ligand variation and how they control emissive phenomena in Ir(III) complexes.[61,62] TD-DFT studies combined with Franck-Condon (FC) emission spectral fitting provide detailed and useful insights into both electronic and molecular structures of complex excited states and provide a basis for experimental data analysis.[29,44]
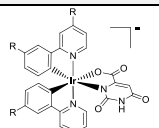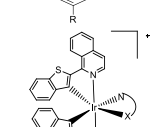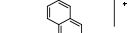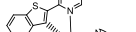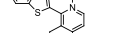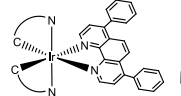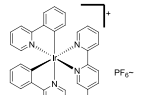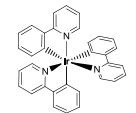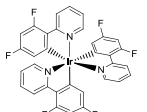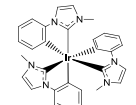
In molecular orbitals (MO) terms, UV-visible transitions in heteroleptic Ir(III) complexes can mostly be ascribed to two main types:[30,34] (1) LC transitions occurring from π to π* orbitals within the same bidentate ligand with a negligible role of the Ir(III) core in the excitation process. Any subsequent photoprocess from LC excitation has excited state characteristics similar to the free-ligand; (2) CT transitions involving electron transfer within the complex can be of two types: i) metal-to-ligand (MLCT) transition, with excitation of a Ir-centered electron to a π* orbital in one of ligands;[5] ii) ligand-to-ligand (LLCT)[62] in heteroleptic complexes from π levels in ligand-A to π* acceptor in ligand-B, with no major role for the Ir-core.

6

Less intense *d-d* transitions are usually not observed in room temperature absorption spectra of Ir(III) complexes because of their overlap with higher energy, far more intense, LC and MLCT transitions.[30]

This *Perspective* is focused solely on heteroleptic [Ir(*Rppy*)$_2$(*L^X*)]$^+$ complexes and arises from our research interest in this area.[28,29,40,41] Table 1 summarizes the photophysical properties of selected compounds published since 2013. These complexes were chosen, based on an extensive literature survey, for showing emission in different color ranges with high quantum yields – important features for exploitation in efficient devices as discussed throughout the manuscript – as well as similar molecular and electronic structures to the compounds investigated by us.[28,29,40,41]

Table 1. Photophysical parameters at 298 K of recently published Ir(III) complexes with suitable features to be exploited in light-emitting devices.

Series entry	Complex		ϕ	λ_{max} / nm	τ / ns	Degassed Solvent	CIE $(x; y)$	Ref.
i		$R_1 = CH_3$; [Ir($Fppy$)$_2$($Mepic$)]	0.98, against fac-[Ir(ppy)$_3$] ($\phi = 0.99$) and [Ir($Fppy$)$_2$(dmb)]$^+$ ($\phi = 0.96$) in CH$_3$CN	474	760	CH$_3$CN	0.14; 0.29	40
		$R_1 = H$; [Ir($Fppy$)$_2$(pic)]	0.89, absolute measurement	471	1700	CH$_2$Cl$_2$	0.15; 0.32	64
			0.83, against fac-[Ir(ppy)$_3$] ($\phi = 0.99$) and [Ir($Fppy$)$_2$($Mepic$)] ($\phi = 0.98$) in CH$_3$CN	470	740	CH$_3$CN	0.14; 0.26	40
			0.63, against [Ir(ppy)$_3$] in CH$_3$CN ($\phi = 0.40$)	472	--	CH$_3$CN	--	65
			0.61	469	1690	CH$_3$CN	--	66
		[Ir($Fppy$)$_2$(dmb)]$^+$	0.96, against [Ru(bpy)$_3$]$^{2+}$ in CH$_3$CN ($\phi = 0.095$) and absolute measurement	522	660	CH$_3$CN	0.26; 0.52	29
		[Ir(ppy)$_2$(dmb)]$^+$	0.28, against coumarin-30 in ethanol ($\phi = 0.81$)	580	530	THF	--	67
			0.23, against [Ru(bpy)$_3$]$^{2+}$ in CH$_3$CN ($\phi = 0.095$) and absolute measurement	580	310	CH$_3$CN	0.49; 0.49	29
			0.22, against [Ru(bpy)$_3$]$^{2+}$ in CH$_3$CN ($\phi = 0.095$)	561	600	CH$_2$Cl$_2$	--	28
		$R_1 = $ phenyl; [Ir(ppy)$_2$(Ph_2phen)]$^+$	0.29, against [Ru(bpy)$_3$]$^{2+}$ in CH$_3$CN ($\phi = 0.095$) and absolute measurement	602	430	CH$_3$CN	0.55; 0.44	29
		$R_1 = H$; [Ir(ppy)$_2$($phen$)]$^+$	0.47, against [Ru(bpy)$_3$]$^{2+}$ in H$_2$O ($\phi = 0.042$)	566	1040	CH$_2$Cl$_2$	--	68
			0.39, absolute measurement	583	230	CH$_3$CN	--	69
			0.27, against [Ru(bpy)$_3$]$^{2+}$ in CH$_3$CN ($\phi = 0.095$) and absolute measurement	590	360	CH$_3$CN	0.52; 0.48	29
		[Ir($Fppy$)$_2$($PhenSe$)]$^+$	0.957, against [Ru(bpy)$_3$]$^{2+}$ in CH$_2$Cl$_2$ ($\phi = 0.029$)	528	463	CH$_2$Cl$_2$	0.30; 0.63	70
ii		R= CF$_3$; [Ir(F_3Op)$_2$(pic)]	0.74, absolute measurement	461, 483	2710	mCPPO1	0.14; 0.16	71
		R= (CF$_2$)$_2$CF$_3$; [Ir(F_7Op)$_2$(pic)]	0.52, absolute measurement	464, 485	2740	films	0.14; 0.17	71
		R= CF$_3$; [Ir(F_3Op)$_2$($fptz$)]	0.63, absolute measurement	446, 470	1460	(50-nm-thick)	0.15; 0.12	71
		R= (CF$_2$)$_2$CF$_3$; [Ir(F_7Op)$_2$($fptz$)]	0.42, absolute measurement	449,474	1540		0.15; 0.13	71
iii		[Ir($FMeppy$)$_2$($2,5$-tpy)]$^+$	0.93, against [Ru(bpy)$_3$]$^{2+}$ in CH$_3$CN ($\phi = 0.095$)	544	1810	CH$_3$CN	0.38; 0.58	72
		[Ir($FMeppy$)$_2$($dmab$)]$^+$	0.74, against quinine sulfate in 0.5 mol L^{-1} H$_2$SO$_4$ ($\phi =0.55$) and [Ru(bpy)$_3$]$^{2+}$ in CH$_3$CN ($\phi = 0.095$)	466, 494, 525	3130	CH$_3$CN	0.19; 0.36	73
iv		[Ir(dpq)$_2$(pic-N-O)]	0.83, against [Ir(piq)$_2$($acac$)] ($\phi = 0.2$)	586	--	CHCl$_3$	0.53; 0.47	74
		[Ir(cpq)$_2$(pic-N-O)]	0.76, against [Ir(piq)$_2$($acac$)] ($\phi = 0.2$)	599	--	CHCl$_3$	0.64 ; 0.36	74

8

Series entry	Complex	ϕ	λ_{max} / nm	τ / ns	Degassed Solvent	CIE (x; y)	Ref.
v	R = H; [Ir(*ppy*)$_2$(*orotate*)]$^-$	0.69, against [Ru(*bpy*)$_3$]$^{2+}$ in H$_2$O (ϕ = 0.028)	530	1090	CH$_3$CN	0.34; 0.62	[53]
	R = CH$_3$; [Ir(*Meppy*)$_2$(*orotate*)]$^-$	0.58, against [Ru(*bpy*)$_3$]$^{2+}$ in H$_2$O (ϕ = 0.028)	536	1142	CH$_3$CN	0.36; 0.61	[53]
vi	[Ir(*btq*)$_2$(*pic*)]	0.12, against *fac*-[Ir(*ppy*)$_3$] in CH$_2$Cl$_2$ (ϕ = 0.40)	698	--	CH$_2$Cl$_2$	0.73; 0.27	[75]
	[Ir(*btq*)$_2$(*dtb*)]$^+$	0.12, against *fac*-[Ir(*ppy*)$_3$] in CH$_2$Cl$_2$ (ϕ = 0.40)	683	--	CH$_2$Cl$_2$	0.73; 0.27	[75]
	[Ir(*btq*)$_2$(*phen*)]$^+$	0.11, against *fac*-[Ir(*ppy*)$_3$] in CH$_2$Cl$_2$ (ϕ = 0.40)	682	--	CH$_2$Cl$_2$	0.73; 0.27	[75]
	[Ir(*btq*)$_2$(*bpy*)]$^+$	0.10, against *fac*-[Ir(*ppy*)$_3$] in CH$_2$Cl$_2$ (ϕ = 0.40)	682	--	CH$_2$Cl$_2$	0.73; 0.27	[75]
vii	[Ir(*pbq-g*)$_2$(*Ph$_2$phen*)]$^+$	0.31, against tetraphenylporphyrin in toluene (ϕ = 0.13), using a Ge detector.	706, 775, 860	--	CH$_3$CN	0.73; 0.27	[76]
		0.03, against tetraphenylporphyrin in toluene (ϕ = 0.13), using a red PMT.	694, 752	1860	CH$_3$CN	--	[76]
		0.035, absolute measurement	698, 760	1860	CH$_2$Cl$_2$	--	[77]
	[Ir(*mpbqx-g*)$_2$(*Ph$_2$phen*)]$^+$	0.19, against tetraphenylporphyrin in toluene solution (ϕ = 0.13), using a Ge detector.	776, 855, 935		CH$_3$CN	0.73; 0.27	[76]
		0.002, against tetraphenylporphyrin in toluene solution (ϕ = 0.13), using a red PMT.	755	350	CH$_3$CN	--	[76]
viii	[Ir(*ppy*)$_2$(*bpyBODIPY*)]$^+$	0.326, against [Ru(*dmb*)$_3$]$^{2+}$ in CH$_3$CN (ϕ = 0.073)	683	--	toluene	0.73 ; 0.27	[78]
		0.013, against [Ru(*dmb*)$_3$]$^{2+}$ in CH$_3$CN (ϕ = 0.073)	716	--	CH$_2$Cl$_2$	--	[78]
		0.006, against [Ru(*dmb*)$_3$]$^{2+}$ in CH$_3$CN (ϕ = 0.073)	718	--	CH$_3$OH	--	[78]
		0.004, against [Ru(*dmb*)$_3$]$^{2+}$ in CH$_3$CN (ϕ = 0.073)	736	--	CH$_3$CN	--	[78]
ix	*fac*-[Ir(*ppy*)$_3$]	0.99, absolute measurement	527	--	CH$_3$CN	0.33; 0.6	[79]
		0.97, absolute measurement	508	1600	2-MeTHF	--	[80]
		0.40, against *fac*-[Ir(*ppy*)$_3$] (ϕ = 0.40)	512	2100	CH$_3$CN	--	[81]
		0.40, against *fac*-[Ir(*ppy*)$_3$] (ϕ = 0.40)	509	340	toluene	--	[82]
	fac-[Ir(*Fppy*)$_3$]	0.99, absolute measurement	495	--	CH$_3$CN	0.18; 0.42	[79]
		0.98, absolute measurement	466	1700	2-MeTHF		[80]
		0.97, absolute measurement	467	1500	CH$_2$Cl$_2$	--	[64]
		0.43, against coumarin-47 in ethanol (ϕ = 0.60)	468	1600	2-MeTHF	--	[56]
		0.43, against *fac*-[Ir(*ppy*)$_3$] (ϕ = 0.40)	472, 492	1600	CH$_3$CN	--	[81]
	fac-[Ir(*pmi*)$_3$]	0.99, absolute measurement	384, 405, 423	--	CH$_3$CN	0.16; 0.04	[79]

Quantum yields are, sometimes, questionable, depending on how well established are the method or the standards used in measurements. The use of proper standards, with similar λ_{em} and ϕ values, is the most important factor as discussed by Brouwer.[83] Absolute measurements (e.g. by using integrating spheres) are usually more reliable, although with associated errors. To avoid misleading comparisons, Table 1 also lists the method and/or standard employed in the ϕ measurements of these complexes.

TD-DFT is an excellent tool for assigning the absorption spectra of [Ir(*NC*)$_2$(*L^X*)] complexes, which can be complicated by overlap with mixed-nature bands. Calculations for a significant number of Ir(III) complexes have shown that the HOMO is a $d_{(Ir)}\pi_{(N^\wedge C)}$ orbital, as depicted in Figure 2A for [Ir(*ppy*)$_2$(*dmb*)]$^+$, with extended electronic interactions between d and π orbitals through the strong Ir(III)-C quasi-covalent bond. Their first lowest-energy singlet transition (S$_1$) results from an orbital promotion from the HOMO to a $\pi^*_{(L^\wedge X)}$ LUMO, and has been assigned to a MLCT state with LLCT mixing.[29,34,40,84] The wave function (Ψ_{S_1}) for these MLCT-based S$_1$ states can be considered as a combination of spin (Ω) and spatial parts (ψ) of the dπ- and $\pi*$-orbital wave functions,[8] Equation 3.

$$\Psi_{S_1} = {}^1\Omega \times \psi_{S_1} = {}^1\Omega \times \frac{1}{\sqrt{2}}\left[\psi_{d_{(Ir)}\pi_{(N^\wedge C)}}(1)\cdot\psi_{\pi^*_{(L^\wedge X)}}(2) + \psi_{d_{(Ir)}\pi_{(N^\wedge C)}}(2)\cdot\psi_{\pi^*_{(L^\wedge X)}}(1)\right] \tag{3}$$
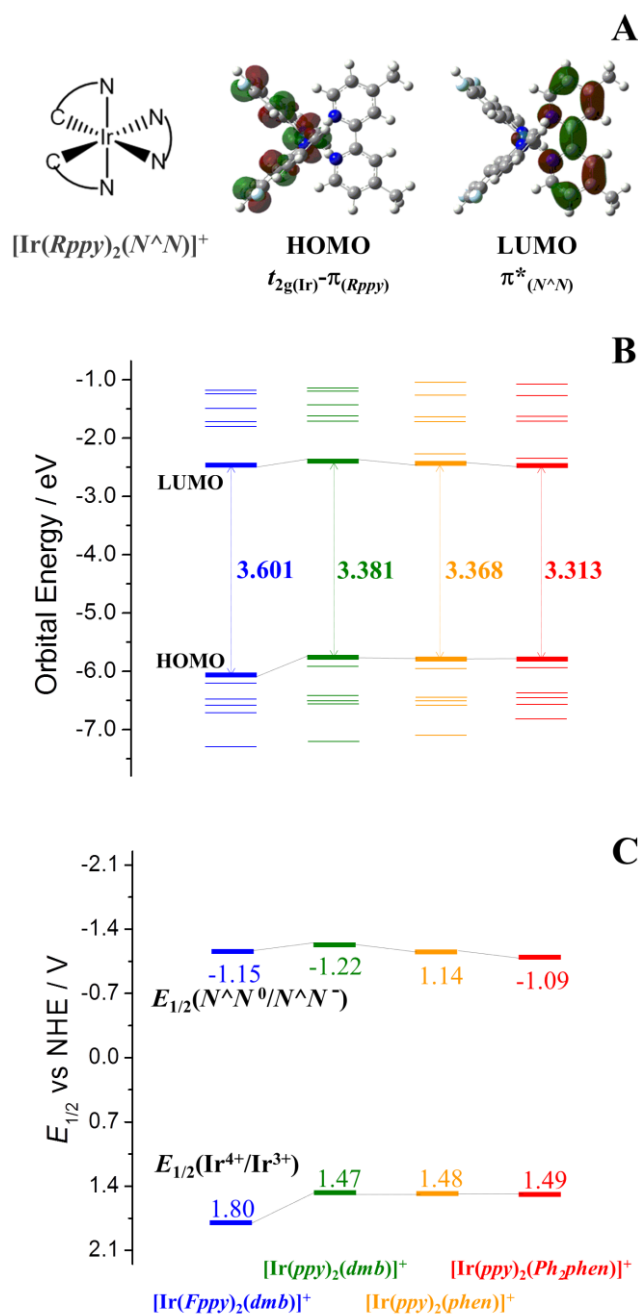
Figure 2. (A) HOMO and LUMO electron contours, (B) orbital energies calculated by TD-DFT and (C) experimental redox potentials for the $[Ir(Rppy)_2(N^\wedge N)]^+$ series. Adapted from reference 29.

In terms of energy modulation, a change in the cyclometallated moiety to more-stable $\pi_{(NC)}$ ligands decreases the $d_{(Ir)}\pi_{(N^\wedge C)}$ HOMO energy, increasing the calculated energy of $d_{(Ir)}\pi_{(N^\wedge C)}\rightarrow\pi^*_{(L^\wedge X)}$ transitions,[32,59] as exemplified by the $[Ir(Rppy)_2(N^\wedge N)]^+$ series, $N^\wedge N =$

polipyridinic ligand, Figure 2B.[29]   For these MLCT-based S_1 states, variations in calculated energies are linearly correlated to differences in redox potentials (ΔE^0), obtained experimentally.[29] In Figure 2C, the Ir-based oxidation ($E^0_{Ir4+/Ir3+}$) shifts anodically from ~1.48 to 1.80 V by adding electron-withdrawing fluorine groups to *ppy*,[29] a change that can lead to large and strategical blue shifts in absorption and emission spectra.[29]

On the other hand, electron-donating groups in the *L^X* moiety increase the S_1 energy by increasing the $\pi^*_{(L^X)}$ LUMO energy. For the [Ir(*Rppy*)$_2$(*NN*)]$^+$ series, Figure 2C, the ligand-based reduction ($E^0_{N^N+/N^N0}$) ranges from −1.09 to −1.22 V by replacing the electron-withdrawing *Ph₂phen* by the electron-donating *dmb* ligand.[29] When the $\pi^*_{(L^X)}$ energy is high enough to overcome the $\pi^*_{(Rppy)}$ energy, S_1 becomes a mixed MLCT/LC$_{Ir(Rppy)\rightarrow Rppy}$ state relative to the Ir-*Rppy* HOMO and a *Rppy* LUMO, as can be observed in the [Ir(*Rppy*)$_2$(*Rpic*)] series, *Rpic* = substituted-picolinate derivatives.[40,48,66] The first three low-lying transitions for [Ir(*Fppy*)$_2$(*Mepic*)], for example, are typically ascribed to MLCT/LC$_{Ir(Fppy)\rightarrow Fppy}$ and MLCT/LLCT$_{Ir(Fppy)\rightarrow Mepic}$.[40]

Triplet states are generated by spin inversion of the single electron in the singly-occupied LUMO of their singlet counterparts. The wave function (Ψ_{T1}) for the triplet counterpart of S_1 is described similarly to Ψ_{S1}, however with inversion in the sign inside the brackets,[8] Equation 4.

$$\Psi_{T_1} = {}^3\Omega \times \psi_{T_1} = {}^3\Omega \times \frac{1}{\sqrt{2}}\left[\psi_{d_{(Ir)}\pi_{(N^C)}}(1)\cdot\psi_{\pi^\bullet_{(L^X)}}(2) - \psi_{d_{(Ir)}\pi_{(N^C)}}(2)\cdot\psi_{\pi^\bullet_{(L^X)}}(1)\right] \tag{4}$$

Formation of a given T_n state is followed by a decrease in the former-S_n energy ($\Delta E_{Sn\text{-}Tn}$) equal to twice the exchange energy ($K_{Sn\text{-}Tn}$), an effect that arises from Coulomb intra- and inter-atomic electron repulsions in the triplet state, Equation 5.[8]

$$\Delta E_{S_1-T_1} = 2K_{S_1-T_1} = 2\iint \psi_{d_{(Ir)}\pi_{(N^C)}}(1)\psi_{\pi^\bullet_{(L^X)}}(1)\frac{e^2}{r_{1,2}}\psi_{d_{(Ir)}\pi_{(N^C)}}(2)\psi_{\pi^\bullet_{(L^X)}}(2)\,dv_1 dv_2 \tag{5}$$

The exchange energy between ^{1}LC and ^{3}LC counterparts is higher than MLCT-based ones,[83] which can lead to close-lying ^{3}LC and ^{3}MLCT states having similar energies.[34] Based

solely on electronic effects, the emissive, low-lying T_1 state can be either MLCT or LC-based excited states, depending on the ligands.

A ^{3}LC emission is usually media-independent and short-lived, with relatively narrow bands in a vibronically resolved spectrum, while the ^{3}MLCT emission, with a microsecond lifetime, results in a broad non-structured spectrum, highly sensitive to the rigidity of the medium. This so-called rigidochromic effect is only observed for dipole-inductive CT transitions. It arises from the response of the surrounding molecules in the medium to the new configuration of the excited state, largely by local medium dipole reorientation.[29,85–88] The reorientation takes place promptly in fluid solutions, yet is restrained in more constricted media, destabilizing the CT state. Similar observations have been reported for series of Re(I), Ru(II) and Os(II) MLCT emitters.[85–87,89,90] Moreover, independent of SOC effects, the momentary dipole of pure MLCT transitions also leads to higher radiative rates, since, as shown in Equation 6, k_r varies by the square of the transition dipole moment ($\vec{M}_{T1}$),[8,29,34,44]

$$k_r = \frac{64\pi^4 n^3}{3\hbar} \left| \vec{M}_{T1} \right|^2 \langle \bar{v}^{-3} \rangle^{-1}$$

(6)

with $\bar{v}$ the average emission energy and n the refraction index of the solvent.

On the other hand, the same trend is not observed for LLCT transitions despite showing relatively large $\vec{M}$, since they are followed by weakening of Ir-C bonds, leading to facilitated non-radiative processes.[34,91]

These spectral characteristics are depicted in Figure 3A. Emission spectra for the [Ir($Rppy$)$_2$($N^\wedge N$)]$^+$ series shown in nitrile solvents at 298 K are broad and media dependent, characteristic of ^{3}MLCT emissions.[29,40] A 80 nm blueshift is observed for [Ir(ppy)$_2$(Ph_2phen)]$^+$ upon cooling to 77 K,[29] consistent with an increase in the MLCT energy by the rigidochromic effect, Figure 3B. As for [Ir($Fppy$)$_2$($Mepic$)], this energy increase is high enough to result in an inversion of the excited state order, with ^{3}MLCT > ^{3}LC, as evidenced by the highly-structured ^{3}LC emission at 77 K,[40] Figure 3B.
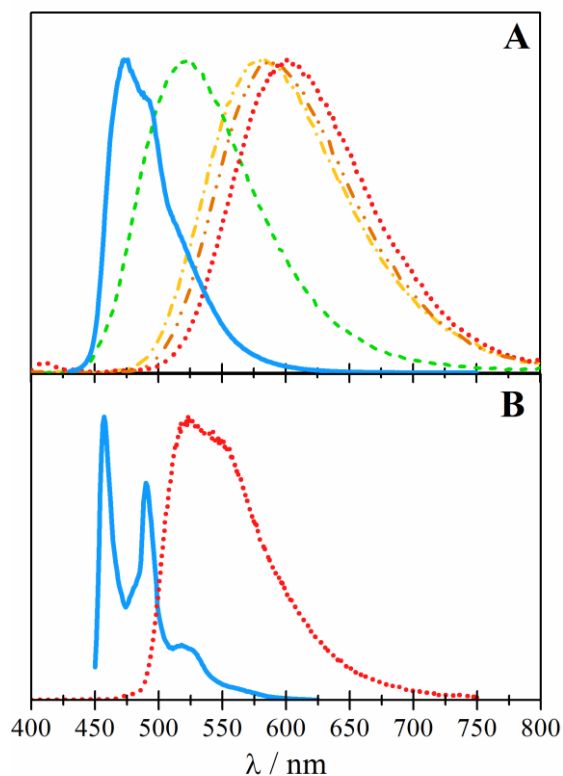
Figure 3. Emission spectra (λ_{ex} = 365 nm) in nitriles at 298 K (A) and 77 K (B) for the [Ir(*Rppy*)$_2$(*L^X*)] series: [Ir(*Fppy*)$_2$(*Mepic*)] (blue —); [Ir(*Fppy*)$_2$(*dmb*)]$^+$ (green − − −); [Ir(*ppy*)$_2$(*dmb*)]$^+$ (yellow –•–•); [Ir(*ppy*)$_2$(*phen*)]$^+$ (orange –••–••) and [Ir(*ppy*)$_2$(*Ph$_2$phen*)]$^+$ (red ••••).

The use of a selenazole as ancillary ligand in the [Ir(*Rppy*)$_2$(*N^N*)]$^+$ series, [Ir(*Fppy*)$_2$(*phenSe*)]$^+$,[70] Table 1(i), results in a ^{3}MLCT$_{Ir(Fppy)\rightarrow phenSe}$ emission in the green, with photophysical parameters comparable to [Ir(*Fppy*)$_2$(*dmb*)]$^+$, with a very high quantum yield for emission of ~0.96. Members of the [Ir(*Fppy*)$_2$(*phenSe*)]$^+$ series have been employed as specific probes for imaging and tracking of mitochondrial structural changes.[70] Anionic [Ir(*Rppy*)$_2$(*orotate*)]$^-$ complexes showed an intense green emission with high quantum yields of 0.58 and 0.69, which are increased to 0.81 and 0.83 for soft salts after coupling to the cationic [Ir(*ppy*)$_2$(*picolylamine*)]$^+$ complex.[53] Phenylquinoline-based Ir(III) complexes, Table 1(iv), such as [Ir(*dpq*)$_2$(*pic-N-O*)] and [Ir(*cpq*)$_2$(*pic-N-O*)], are other recently reported examples of highly emissive compounds with an intense ^{3}MLCT yellow emission.[74]

However, judging the electronic character on the emitting T_1 states (mostly LC or MLCT) for most Ir(III) complexes is difficult since SOC also induces an electronic mixing between MLCT and LC states.[30] Room temperature emissions for [Ir(*Fppy*)$_2$(*Rpic*)][40,64–66,92], [Ir(*FMeppy*)$_2$(*dmab*)]$^+$ [73] and [Ir(*F$_x$Op*)$_2$(*N^X*)],[71] *F$_x$Op* = perfluorocarbonyl phenylpyridine derivatives, Table 1(i-iii), for example, are long-lived (a MLCT characteristic) with vibronically resolved spectra (a LC characteristic), as depicted for [Ir(*Fppy*)$_2$(*Mepic*)] in Figure 3A. The synthesis, structural characterization and key emission properties of the archetypal [Ir(*Fppy*)$_2$(*pic*)] complex were recently reviewed.[93]

SOC-mixing has been described by Group Theory, as demonstrated in subsequent discussions for [Ir(*ppy*)$_2$(*N^N*)]$^+$ complexes (*N^N* = polipyridinic ligands, which are $^3B_2$ molecules in a C_{2v} point symmetry),[94] with similar approaches viably extended to most heteroleptic [Ir(*N^C*)$_2$(*L^X*)] compounds. Following the arguments of Komada et al.,[95] who adopted the mono-chelated complex approximation to assign the symmetry and sublevel ordering of mixed-T_1 states in [Rh(*N^N*)$_3$]$^{3+}$ complexes, the zero-field splitting of the lowest-lying $\pi \rightarrow \pi^*$ transition in free *N^N* ligands are accounted as A_1, A_2 and B_1 irreducible representations. After coordination to Ir(*ppy*)$_2$, the C_{2v} symmetry is retained, restricting the three viable $d\pi \rightarrow \pi^*$ MLCT sublevels as B_1, B_2 and A_1. For [Ir(*N^C*)$_2$(*N^N*)]$^+$ complexes, MLCT and LC sublevels of the same representation (A_1 and B_1) are those capable of undergoing SOC-induced mixings.

In a simplistic two-electron approximation, the SOC operator (H_{SO}) can be expressed by Equations 7a and 7b,[5]

$$H_{SO} = \vec{B}_1 \vec{s}_1 + \vec{B}_2 \vec{s}_2 \tag{7a}$$

$$H_{SO} = \frac{1}{2}\left(\vec{B}_1 + \vec{B}_2\right)\left(\vec{s}_1 + \vec{s}_2\right) + \frac{1}{2}\left(\vec{B}_1 - \vec{B}_2\right)\left(\vec{s}_1 - \vec{s}_2\right) \tag{7b}$$

where $\vec{s}_i$ is the spin angular momentum operator and $\vec{B}_i$ is a function of the SOC constant (ζ) and the orbital operator ($\vec{l}_i$), Equation 8.

$$\vec{B}_i = \frac{e^2 \hbar^2}{2m^2 c^2} \sum \frac{Z_{eff}}{r^3} \times \vec{l}_i = \zeta \times \vec{l}_i \tag{8}$$

In this treatment, H_{SO} consists of a product of both spatial and spin parts. The first product in Equation 7B is the symmetrical electron permutation that can mix two different states with the same multiplicity while the second is the opposite, asymmetrical interaction between singlet and triplet states.

The degree of mixing in Ψ_{T1} can be estimated by accounting for the spatial parts of the two states-of-origin (*a* and *b*, where *a* is dominant),[8,94] Equation 9.

$$\Psi_{T_1} = \sqrt{1 - \beta_{a-b}^2}\,|a\rangle + \beta_{a-b}\,|b\rangle \tag{9}$$

$$\beta_{a-b} = \frac{\langle\psi_a|H_{SO}|\psi_b\rangle}{(\Delta E_{a-b})} \tag{10}$$

with $\Delta E_{a\text{-}b}$ the zero-order energy difference between *a* and *b*.

In considering triplet/singlet mixings, direct SOC between low-lying-^{3}MLCT and ^{1}MLCT states is only feasible if the transitions result from different orbitals having different d-orbitals, as demonstrated by Yersin et al.[96] As for a low-lying ^{3}LC state, ^{3}LC/^{1}MLCT permutations are possible only indirectly in a more complex, two-step mechanism, involving a ^{3}LC/^{3}MLCT configuration interaction (CI, supported by molecular-orbital theory) followed by spin-orbit coupling with ^{1}MLCT. Of special note for Ir(III) complexes, the ^{3}LC/^{3}MLCT is usually very effective, assuming a significant interaction between d and π orbitals through the strong organometallic Ir-C bond.

Photophysical elucidations of heavy-metal complexes, such as Re(I), Rh(III) and Ir(III), have widely incorporated triplet/singlet mixing by perturbation theory.[8,84,94–102] This approach dates back 1986, when Komada et al.[95] proposed the symmetry assignment and a model to explain enhanced absorptivities for spin-forbidden triplet bands of $[Rh(bpy)_3]^{3+}$ and $[Rh(phen)_3]^{3+}$ in frozen media, ascribing them to ^{3}LC/^{1}MLCT mixed-states. The triplet/singlet coupling model has been properly extended to discuss the emission of Ir(III) complexes,[34] yet more-detailed photophysical discussions through a complementary account of the triplet/triplet permutation effect is also valuable, in particular for compounds with low-lying ^{3}LC states.

For a low-lying ^{3}MLCT state undergoing ^{3}MLCT/^{1}MLCT or ^{3}MLCT/^{3}LC mixings, for example, Equation 10 can be rewritten as Equations 11a-b by assuming both interactions individually.

$$\beta\,^3_{MLCT-\,^1MLCT} = \frac{\langle\,^3\psi_{MLCT}|H_{SO}|\,^1\psi_{MLCT}\rangle}{\left(\Delta E\,^3_{MLCT-\,^1MLCT}\right)}$$

(11a)

$$\beta\,^3_{MLCT-\,^3LC} = \frac{\langle\,^3\psi_{MLCT}|H_{SO}|\,^3\psi_{LC}\rangle}{\left(\Delta E\,^3_{MLCT-\,^3LC}\right)}$$

(11b)

SOC-permutations result in energy stabilization, which is related to the square of β, presumably with ^{3}MLCT/^{3}LC dominant as a simple consequence of the smaller $\Delta E_{3MLCT-3LC}$ energy gap as compared to $\Delta E_{3MLCT-1MLCT}$,[96] Figure 4.
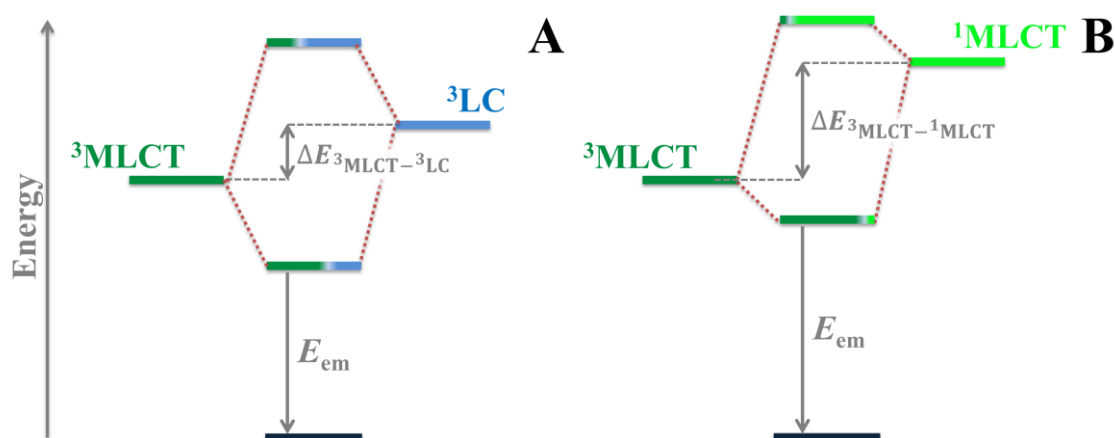
Figure 4. Individual representations of ^{3}MLCT/^{3}LC (A) and ^{3}MLCT/^{1}MLCT (B) SOC-induced permutations.

The dipole moment for a hybrid-T_1 state is better expressed by including SOC effects, as shown in Equation 12, where a and b are the two permuted states. For a more detailed version of Equation 12 and a deeper understanding of individual triplet substates, the reader is referred to the perspective on phosphorescent-OLED mechanisms by Minaev et al.[8] or to the review on triplet states of organometalic compounds by Yersin et al.[96]

$$M_{T_1} = \langle\psi_a|M|\psi_{S_0}\rangle \times \beta_{a-b}$$

(12)

From the relationship of k_r, $\beta_{a\text{-}b}$ and M_{T1} (Equations 6, 10 and 12), more intense T_1 emissions result from increased perturbations arising from smaller $\Delta E_{a\text{-}b}$ values and enhanced MLCT mixing.

Equation 12 is usually expressed in the form of Equation 13 with ^{3}MLCT/^{1}MLCT mixing, since ^{3}MLCT/^{3}LC mixing occurs between spin-forbidden states, leading to a minor contribution to the corresponding dipole matrix elements.[96]

$$M_{T_1} = \langle \psi_{1\text{MLCT}} | M | \psi_{S_0} \rangle \times \beta \, ^3_{\text{MLCT}-\,^1\text{MLCT}}$$

(13)

As described by Equation 13, triplet/singlet mixings are responsible for increased absorptivities for normally spin-forbidden triplet absorptions with enhanced oscillator strengths.

To illustrate coupling effects on emission from Ir(III) complexes, an energy diagram for a [Ir($RFppy$)$_2$($N^\wedge N$)]$^+$ series is proposed, Figure 5. It is based on photoluminescence spectral data at 298 and 77 K available in the literature.[29,72,73] The diagram relies on ^{3}MLCT/^{3}LC configuration interaction and emphasizes individual energies of former ^{3}LC$_{N^\wedge N}$ and ^{3}MLCT$_{\text{Ir(ppy)} \to N^\wedge N}$ counterparts, with their acceptor orbitals at the auxiliary $N^\wedge N$ ligand (i.e. $d\pi^1_{(ppy)} \to \pi^{*1}_{(N^\wedge N)}$ and $\pi^1_{(N^\wedge N)} \to \pi^{*1}_{(N^\wedge N)}$ transitions). A similar approach was recently proposed by our group in the photophysical elucidation of the complex [Ir($Fppy$)$_2$(dmb)]$^{+}$.[29]
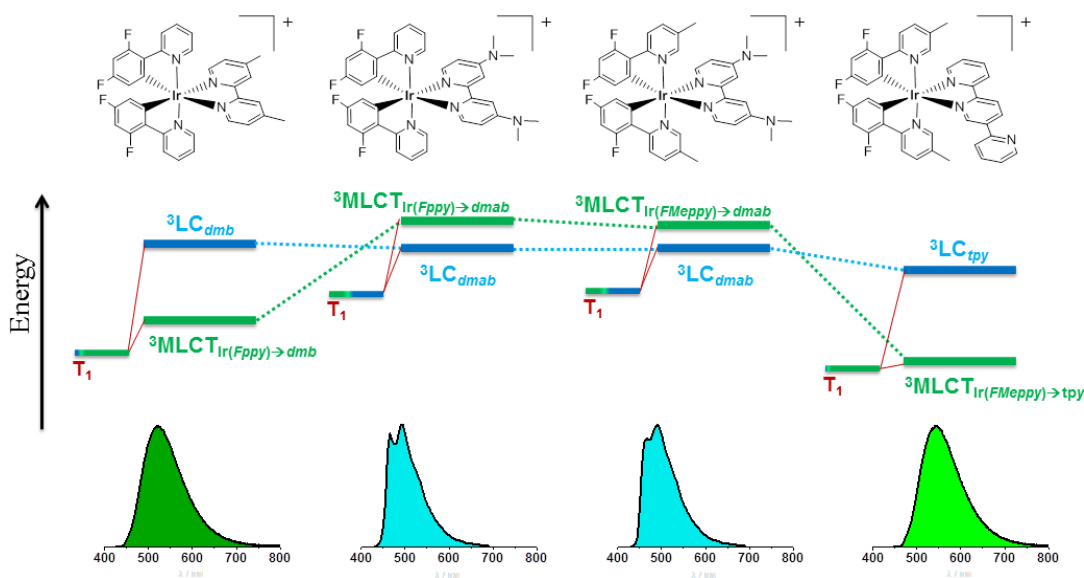

Figure 5. Energy diagram and ^{3}MLCT/^{3}LC configuration interactions for the [Ir($RFppy$)$_2$($N^\wedge N$)]$^+$ series and 298 K spectra from T_1 emissive decays.

The mixed T_1 state of the blue-green [Ir(*Fppy*)$_2$(*dmb*)]$^+$ complex possesses majority MLCT character, with a broad spectrum (λ_{max} = 522 nm) and remarkable k_r value (15 × 10^5 s^{-1}).[29,40] On the other hand, the 298 K spectrum for [Ir(*Fppy*)$_2$(*dmab*)]$^+$ is ~60 nm blueshifted as a result of the strong electron-donating dimethylamino groups, which destabilize the ^{3}MLCT$_{Ir(Fppy) \to N^\wedge N}$ energy, while ^{3}LC$_{dmb}$ and ^{3}LC$_{dmab}$ energies are similar.[73] The ^{3}MLCT destabilization is high enough to invert the energy order and the ^{3}LC$_{dmab}$ counterpart plays a major role in the T_1 mixed-nature of [Ir(*Fppy*)$_2$(*dmab*)]$^+$.[73] The LC inversion decreases k_r (2.0 × 10^5 s^{-1}) and leads to a vibronically resolved emission spectrum, with similar spectral profile to the free *dmab* ligand. Using molecular engineering strategies, the k_r value can be further tuned by the addition of a methyl group in the *Fppy* moiety ([Ir(*FMeppy*)$_2$(*dmab*)]$^+$) that stabilizes the ^{3}MLCT counterpart, decreasing the energy difference towards the low-lying ^{3}LC counterpart,[73] which slightly enhances the MLCT influence in the mixed T_1 state, leading to a slightly higher k_r (2.3 × 10^5 s^{-1}) and a minor spectral redshift of 4 nm. An additional replacement of the ancillary *dmab* ligand to the electron-withdrawing 2,2':5,2"-terpyridine ligand ([Ir(*FMeppy*)$_2$(*2,5-tpy*)]$^+$) further decreases the MLCT energy, restoring the energy order (MLCT < LC), resulting in a broad redshifted (λ_{max} = 544 nm) spectrum and a higher k_r (5.1 × 10^5 s^{-1}), although smaller than [Ir(*Fppy*)$_2$(*dmb*)]$^+$ due to lower state mixing through a higher $\Delta E_{MLCT-LC}$.[72] The diagram also depicts the difficulty in obtaining blue emitters with a high k_r since the MLCT destabilization increases the energy difference towards the LC state, leading to a greater influence of the LC counterpart in blue-emissive T_1 states.

As for T_1 states, which are mainly governed by non-radiative decays (vibrational decay), the Energy Gap Law properly relates k_{nr} and the emission energy (E_{em}).[44] The relationship is expressed by Equation 14 for a single-promoting mode of quantum spacing $\hbar\omega_M$ within a weak vibrational coupling limit (with $E_{em} >> S_M\hbar\omega_M$ and $\hbar\omega_M >> k_BT$).[44] A more complete expression with multiple modes is required in order to reconcile deviations from the single-mode treatment.

$$\ln k_{\rm nr} = \ln \frac{\sqrt{2\pi}}{\hbar} \frac{V_{\rm k}^2}{(1000~{\rm cm}^{-1})} - \frac{1}{2}\ln\left[\frac{\hbar\omega_{\rm M} E_{\rm em}}{(1000~{\rm cm}^{-1})^2}\right] - S_{\rm M} - \frac{\gamma_0 E_{\rm em}}{\hbar\omega_{\rm M}} + \frac{(\gamma_0+1)^2}{\hbar\omega_{\rm M}}\left(\frac{\tilde{v}_{1/2}}{16\ln 2}\right)^2 \quad (14a)$$

$$\gamma_0 = \ln\left(\frac{E_{em}}{S_{\rm M}\hbar\omega_{\rm M}}\right) - 1 \quad\quad\quad (14b)$$

In Equation 15, $E_{\rm em}$ is approximately equal to the energy gap between the zeroth vibrational levels in the ground and excited states (E_0), $S_{\rm M}$ is the electron-vibrational coupling constant associated to $\hbar\omega_{\rm M}$, $\tilde{v}_{1/2}$ is the fwhm for an individual vibronic line and $V_{\rm k}$ is the vibrationally induced electronic coupling matrix element. Their values are obtained by Franck-Condon (FC) emission spectral fittings[29,40,103,104] and application of the Golden Rule, as reported by Ito and Meyer.[44]

Equation 14 predicts increased nonradiative decays for lower-energy T_1 states, hence red-emissive compounds (lower $E_{\rm em}$) are usually less efficient as emitters. Some complexes reported recently present promising strategies for leading to efficient red emitters and are listed in Table 1. The use of 1-(benzo[b]thiophen-2-yl)isoquinoline as a cyclometallated ligand in the [Ir(*btq*)$_2$(L^X)] series, Table 1(vi), leads to red ^{3}MLCT$_{\rm Ir(btq)\to L^X}$ emission, with moderate quantum yields ($\phi \sim 0.12$).[75] The phenylbenzo[g]-quinoline ligand in [Ir(*pbq-g*)$_2$(*Ph$_2$phen*)]$^+$, Table 1(vii), also results in a red emission, and a further redshift to the near infrared is observed after addition of an electron-withdrawing sp^2-N opposite to the chelating N atom in [Ir(*mpbqx-g*)$_2$(*Ph$_2$phen*)]$^+$.[76,77] Another interesting strategy is the use of *styryl-BODIPY* ancillary ligands to harvest red and near infra-red light through π-conjugated linkers that ensure efficient intersystem crossing to long-lived emissive ^{3}LC$_{BODIPY}$ states.[78] In a recent work, the [Ir(*ppy*)$_2$(*bpyBODIPY*)]$^+$ complex, Table 1(viii), was employed as a multi-functional material in luminescent bioimaging and intracellular photodynamic studies.[78]

In terms of the emission, infinite scales of color and tonalities are possible to be perceived by the human eye vision. The Comission Internationale d'Eclairage (CIE) quantified the color perceived by humans in three matching functions or spectral sensitivity curves ($\bar{x}(\lambda)$, $\bar{y}(\lambda)$ and $\bar{z}(\lambda)$) based on trichromatic stimuli of the human virtual cortex.[105,106] The numerical values of these standard matching functions are available as free-access tables.[107] In this *Perspective*, we normalized the photoluminescence spectral data of the complexes listed in

Table 1 by the use of Equations 15a-c and calculated their photoluminescence CIE coordinates

(x and y) using Equations 16a-b, leading to the 2D color space chromaticity diagram in Figure 6.

$$X = \int_{380}^{780} I(\lambda)\bar{x}(\lambda)d\lambda \tag{15a}$$

$$Y = \int_{380}^{780} I(\lambda)\bar{y}(\lambda)d\lambda \tag{15b}$$

$$Z = \int_{380}^{780} I(\lambda)\bar{z}(\lambda)d\lambda \tag{15c}$$

$$x = \frac{X}{X+Y+Z} \tag{16a}$$

$$y = \frac{Y}{X+Y+Z} \tag{16b}$$

1.	[Ir(*Fppy*)₂(*Mepic*)]	10.	[Ir(*cpq*)₂(*pic-N-O*)]
2.	[Ir(*Fppy*)₂(*pic*)]	11.	[Ir(*FMeppy*)₂(2,5-tpy)]⁺
3.	[Ir(*Fppy*)₂(*dmb*)]⁺	12.	[Ir(*FMeppy*)₂(*dmab*)]⁺
4.	[Ir(*ppy*)₂(*dmb*)]⁺	13.	[Ir(*btq*)₂(*N^X*)]
5.	[Ir(*ppy*)₂(*Ph₂phen*)]⁺	14.	[Ir(*N^C*)₂(*Ph₂phen*)]⁺
6.	[Ir(*ppy*)₂(*phen*)]⁺	15.	[Ir(*ppy*)₂(*bpyBODIPY*)]⁺
7.	[Ir(*Fppy*)₂(*PhenSe*)]⁺	16.	*fac*-[Ir(*ppy*)₃]
8.	[Ir(*FₓOp*)₂(*N^X*)]	17.	*fac*-[Ir(*Fppy*)₃]
9.	[Ir(*dpq*)₂(*pic-N-O*)]	18.	*fac*-[Ir(*pmi*)₃]
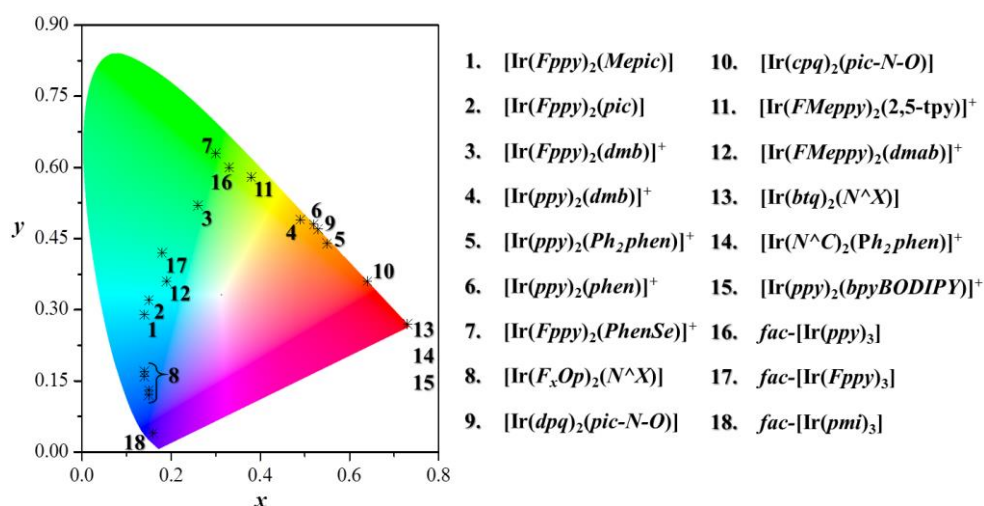
Figure 6. Color space chromaticity diagram with CIE coordinates for the photoluminescence of

Ir(III) complexes listed in Table 1.

Photoluminescence CIE coordinates are very useful for an absolute assessment and a

quantitative comparison among emission colors of different compounds, yet underused for

photoluminescence. The compounds listed in Table 1 present emission in many different colors

and tonalities, exemplifying the outstanding color tuning offered by Ir(III) complexes via

molecular engineering. Moreover, for the pursuit and design of white-emitting systems, the CIE

diagram can identify emissions in complementary colors, since paired compounds are connectable by a direct line crossing through the "pure white" region at the center (around $x = 0.33$; $y = 0.33$). For example, the use of blue [Ir($Fppy$)$_2$($Mepic$)] ($x = 0.14$; $y = 0.29$) and orange-red [Ir(cpq)$_2$(pic-N-O)] ($x = 0.64$; $y = 0.36$) compounds in the active layers of emitting devices can result in white-light emitting systems.

LIGHT-EMITTING DEVICES

The beginning of the LED history dates from 1907, when Round[108] reported, for the first time, the electroluminescence (EL) of SiC (carborundum) after application of current. The emission process was not well understood, and the LED was described as a Schottky diode rather than a p-n junction diode. Not until 1928 did Lossev[109] describe the SiC high-field luminescence phenomenon.[110–113] In 1936, Destriau[114] observed a light emission from a Cu-doped ZnS thin layer upon application of AC voltage.[110,111,115,116] The first EL device, based on GaAsP junctions, with red emission,[117,118] was only reported in 1962 by Holonyak and Bevacqua.[119] In subsequent decades, commercial LEDs in different colors were developed, such as green (nitrogen-doped GaP),[113,120] yellow (nitrogen-doped GaAsP)[113,121] and, in the 90's, blue (GaN:GaInN),[122,123] which can lead to the white light emission. For these discoveries of blue-emitting systems, with energy- and cost-savings, Akasaki, Amano and Nakamura were honored with the 2014 Nobel Prize in Physics.[124]

Organic unsaturated polymers and crystals can also be considered semiconductors due to delocalized π-electrons,[125] with their HOMO and LUMO analogous to valence and conduction bands. Fluorescent deactivation from S_1 is usually observed after external (photo or electrical) excitation of these organic polymers.[8] In particular, the organic semiconductor electroluminescence, firstly detected in 1963 by Pope et al.,[5,8,126,127] is usually observable in thin films (~100 nm) assembled in a sandwich type architecture between a metallic cathode (usually aluminum, gold, or alkali-earth metals) and a transparent conducting oxide anode. The use of conductive and blocking multilayers can promote efficient charge transfer to the emissive thin film in a device.[7,8,128] Application of an external bias leads to electron and hole injection in the

cathode and anode, respectively. After percolating electron/hole conducting/blocking layers, they reach the active film where their close-distance interaction produces excitons, which recombine with light emission.[7,8,128] When OLEDs are operating, the statistic ratio of triplet and singlet excitons formed under electrical excitation is 3:1, since injected electrons and holes have arbitrary spin and are not spin-correlated.[5,96] Therefore, the luminescence efficiency of fluorescent organic devices is limited by only singlet excitons because they show a rather restricted selection rule for singlet-triplet transitions.[129–131]

Only in 1998 did Forrest and Thompson[130] develop an innovative approach by using phosphorescent neutral complexes in OLEDs to reach high efficiencies by full use of singlet and triplet excitons. OLEDs based on triplet emitter complexes (guest) in polymer (host) overcome the S-T selection rule by harvesting emission from both singlet and triplet states, leading to remarkable improvements in their luminescent efficiencies.[5,8,96] For Ir(III) phosphors, in which the SOC effect plays a major role in their excited states, the external efficiency of the electroluminescent device is almost 100%.

In these Ir(III)-polymer (guest-host) based devices, the polymer must efficiently convey its excitation energy to the T_1 excited-state of the emissive Ir(III) complex. There are two main mechanisms of non-radiative energy transfer,[5,8] Förster and Dexter. Förster[132] is a long-range coulombic interaction through a host-to-guest electromagnetic-induced dipole oscillation and a crucial parameter is a significant spectral overlap between host-emission and guest-absorption. According to Förster, excitation of the guest only leads to singlet excited-states because it is dependent on spin-allowed transitions. On the other hand, Dexter[133] transfer is a short-range exchange interaction through an orbital overlap between host and guest and can be applied for both spin-allowed and forbidden transitions. A third mechanism, known as direct charge-trap, is also possible when the HOMO and LUMO energies of both guest and host are comparable.[5,134] The charge-trap mechanism is not necessarily an energy transfer process since excitons, both singlet and triplet, are directly generated in the guest and the host works solely as a charge carrier.

[Ir(*Fppy*)$_2$(*pic*)], *fac*-[Ir(*pmi*)$_3$], *fac*-[Ir(*Fppy*)$_3$] complexes are vastly employed as standard compounds in blue OLEDs, with many examples in the literature. By addition of a methyl group to the *pic* moiety in [Ir(*Fppy*)$_2$(*pic*)], the novel [Ir(*Fppy*)$_2$(*Mepic*)] complex has been engineered as another alternative to efficient blue emitter for OLEDs.[40] A device was recently fabricated in a simple FTO/PEDOT:PSS/PVK:complex/Al architecture (PVK = polyvinylcarbazole) and led to an intense blue-emission, as depicted in Figure 7A.[135] Similarly, [Ir(*F$_x$Op*)$_2$(*L^X*)]-doped organic films were employed as active layers in deep-blue OLEDs, resulting in some of the deepest blue emissions ever achieved and high external quantum (EQE = 17%) and current (CE = 21.7 cd A^{-1}) efficiencies.[71] Recently, phenylquinoline-based Ir(III) complexes, Table 1(iv), such as [Ir(*dpq*)$_2$(*pic-N-O*)] and [Ir(*cpq*)$_2$(*pic-N-O*)], were employed in solution-processed orange OLEDs, which combined low fabrication costs and high CEs (26.9 and 18.1 Cd A^{-1}) and EQEs (14.2 and 11.9%).[72] Near infrared OLEDs fabricated by using [Ir(*pbq-g*)$_2$(*Ph$_2$phen*)]$^+$ and [Ir(*mpbqx-g*)$_2$(*Ph$_2$phen*)]$^+$, however, showed low external efficiencies (0.65 and 0.30%).[76] Although designed for other applications, [Ir(*btq*)$_2$(*L^X*)] and [Ir(*ppy*)$_2$(*bpyBODIPY*)]$^+$ complexes[75,78] might also be an alternative for near infrared emitting devices as well as [Ir(*Rppy*)$_2$(*orotate*)]$^-$ complexes as interesting alternatives to enhance the stability of OLEDs based on anionic emitters.[53]
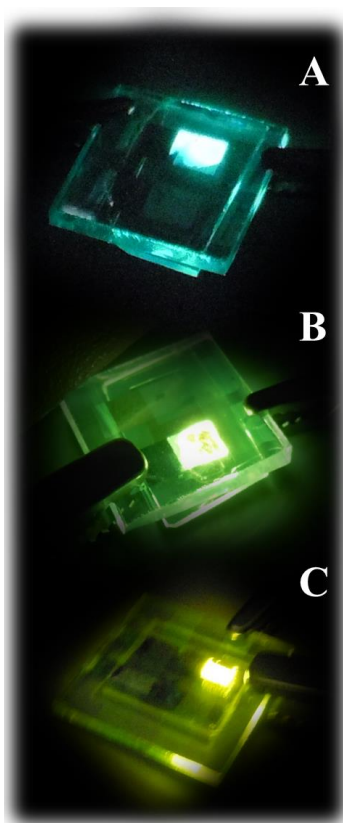
Figure 7. Blue, green and yellow electroluminescence from light-emitting devices based on [Ir(*Fppy*)$_2$(*Mepic*)] (A), [Ir(*Fppy*)$_2$(*dmb*)]$^+$ (B) and [Ir(*ppy*)$_2$(*dmb*)]$^+$ (C).

A slight modification on the working mechanism of OLEDs by using highly concentrated mobile ions (lithium triflate) in the organic active layer led to the development of the first LEC by Pei et al., in 1995.[136] The use of mobile ions drastically changes the operating mechanism and properties of the device,[137,138] allowing simpler architectures.[10] In LECs, after a charge redistribution driven by an applied external bias, injection of holes and electrons leads to electrochemical oxidation and reduction of the polymer.[139–141] Mobile ions with opposite charges stabilize oxidized and reduced species, which recombine to regenerate the original polymer leading to a photon emission. The same approach can be exploited for thin films of solely ionic transition-metal complexes (iTMC),[28,137,142] with the advantage of the ionic complex being responsible for both ionic conductivity and photon emission, requiring only a single active layer. The first work using iTMC as emissive species in LECs was carried out by Lee et al., in 1996.[143] The simplicity and considerable efficiency of the devices make them highly

desirable for cost saving fabrication and sustainable energy source. The majority of the complexes were based on Ru(II); however, nowadays, the use of Ir(III) compounds has been widely emphasized.[144] The progress on increasing iTMC LEC performances in terms of turn-on time, stability and efficiency was recently reported in a complete review.[144]

Concerning iTMC LECs, all complexes in the [Ir($Rppy$)$_2$($N^\wedge N$)]$^+$ series, Table 1(i), present desired characteristics for active layers due to their appropriate photophysical features and high solubility in benign solvents, essential for solution processable depositions (e.g. printing, layer-by-layer and spin-coating).[72,144] [Ir(ppy)$_2$(bpy)]$^+$ and [Ir(ppy)$_2$($phen$)]$^+$ have been used as active layer for the development of distinctive LEC architectures. For instance, the use of these complexes and ionic liquids in the active layers in proof-of-concept LECs leads to remarkable improvements on their turn-on time and power efficiency.[145] Recently, a thin film of the [Ir(ppy)$_2$(dmb)]$^+$ complex in a FTO/PEDOT:PSS/complex/Al architecture demonstrated a very-high current efficiency of 59.7 Cd A^{-1} in a yellow electroluminescence,[28] Figure 7C. Further molecular-engineering led to the [Ir($Fppy$)$_2$(dmb)]$^+$ complex that showed an intense green-electroluminescence in a similar device architecture, Figure 7B.[135] By analogy, [Ir($Fppy$)$_2$($phenSe$)]$^+$ (having λ_{em}, ϕ and T$_1$ values comparable to [Ir($Fppy$)$_2$(dmb)]$^+$) also shows potential applicability in LECs. However, high quantum yields are not enough to guarantee desirable device characteristics since some compounds, for example [Ir($FMeppy$)$_2$($2,5$-tpy)]$^+$,[72] give highly unstable and short-lived devices due to adventitious ligand-exchange reactions. To avoid this effect, the use of an intramolecular cage with bulky substituent groups or ligands capable of intramolecular π-π stacking to shield the Ir metal core lead to remarkable improvements in stability.[69,144] Therefore, [Ir(pbq-g)$_2$(Ph_2phen)]$^+$ and [Ir($mpbqx$-g)$_2$(Ph_2phen)]$^+$, employed in low external efficiency OLEDs, as discussed above, might also result in more efficient lighting systems as LECs.

FINAL REMARKS

The summary of successful molecular engineering in Ir(III) complexes and the many applications in light-emitting systems cited here are inspiring and illustrate the fascinating

26

strategies that are used to understand and design highly emissive compounds. As demonstrated in this *Perspective*, theoretical results based on TD-DFT calculations and the application of the Golden Rule give fundamental support to elucidate photophysical dynamics. The use of combined experimental (sometimes, not properly addressed) and theoretical aspects can lead to a comprehensive understanding of the molecular mechanisms that result in luminescence, the key element in the design of photoluminescent compounds with desired properties that can lead to more efficient lighting-devices.

Future molecular design strategies must head beyond energy and color control. A judicious engineering of MLCT/LC excited state mixing is fundamental for obtaining desired emission energies, spectral shapes, media interactions, and high quantum yields. In the pursuit of smart white-emitting systems, the design of more-efficient red (low-energy gap) and blue emitters (limited by a decreased MLCT influence), is of great interest. The use of photoluminescence CIE coordinates, although underutilized, is a great tool for identifying paired compounds for use in light-emitting devices and modulating their electroluminescence towards desired colors.

ACKNOWLEDGEMENT

AUTHOR INFORMATION

Corresponding Author

* E-mail: neydeiha@iq.usp.br

Author Contributions

R.C.A. and R.L.C. have performed the bibliographical revision; K.P.S.Z., R.C.A, and R.L.C. have calculated CIE coordinates; K.P.S.Z. and N.Y.M.I. have written the manuscript and all authors have reviewed and given approval to its final version.

Notes

The authors declare no competing financial interest.

REFERENCES

1   F. M. Steranka, J. Bhat, D. Collins, L. Cook, M. G. Craford, R. Fletcher, N. Gardner, P. Grillot, W. Goetz, M. Keuper, R. Khare, A. Kim, M. Krames, G. Harbers, M. Ludowise, P. S. Martin, M. Misra, G. Mueller, R. Mueller-Mach, S. Rudaz, Y. C. Shen, D. Steigerwald, S. Stockman, S. Subramanya, T. Trottier and J. J. Wierer, *Phys. Status Solidi Appl. Res.*, 2002, **194**, 380.

2   E. F. Schubert and J. K. Kim, *Science*, 2005, **308**, 1274.

3   E. F. Schubert, J. K. Kim, H. Luo and J.-Q. Xi, *Reports Prog. Phys.*, 2006, **69**, 3069.

4   M.-H. Chang, D. Das, P. V. Varde and M. Pecht, *Microelectron. Reliab.*, 2012, **52**, 762.

5   R. C. Evans, P. Douglas and C. J. Winscom, *Coord. Chem. Rev.*, 2006, **250**, 2093.

6   D. Fyfe, *Nat. Photonics*, 2009, **3**, 453.

7   C.-L. Ho and W.-Y. Wong, *New J. Chem.*, 2013, **37**, 1665.

8   B. Minaev, G. Baryshnikov and H. Agren, *Phys. Chem. Chem. Phys.*, 2014, **16**, 1719.

9   Z. Yu, L. Li, H. Gao and Q. Pei, *Sci. China Chem.*, 2013, **56**, 1075.

10   S. B. Meier, D. Tordera, A. Pertegás, C. Roldán-Carmona, E. Ortí and H. J. Bolink, *Mater. Today*, 2014, **17**, 217.

11   H.-C. Su and C.-Y. Cheng, *Isr. J. Chem.*, 2014, **54**, 855.

12   H.-C. Su and J.-H. Hsu, *Dalton Trans.*, 2015, **44**, 8330.

13   C. Ulbricht, B. Beyer, C. Friebe, A. Winter and U. S. Schubert, *Adv. Mater.*, 2009, **21**, 4418.

14   K. K.-W. Lo, S. P.-Y. Li and K. Y. Zhang, *New J. Chem.*, 2011, **35**, 265.

15   Y. You and W. Nam, *Chem. Soc. Rev.*, 2012, **41**, 7061.

16   K. K.-W. Lo, A. W.-T. Choi and W. H.-T. Law, *Dalton Trans.*, 2012, **41**, 6021.

17   K. K.-W. Lo and K. Y. Zhang, *RSC Adv.*, 2012, **2**, 12069.

18   Y. You, S. Cho and W. Nam, *Inorg. Chem.*, 2014, **53**, 1804.

19   E. Baranoff, J.-H. Yum, M. Graetzel and M. K. Nazeeruddin, *J. Organomet. Chem.*, 2009, **694**, 2661.

20   Z. Ning, Q. Zhang, W. Wu and H. Tian, *J. Organomet. Chem.*, 2009, **694**, 2705.

21   S. Fantacci and F. De Angelis, *Coord. Chem. Rev.*, 2011, **255**, 2704.

22   Y.-J. Yuan, J.-Y. Zhang, Z.-T. Yu, J.-Y. Feng, W.-J. Luo, J.-H. Ye and Z.-G. Zou, *Inorg. Chem.*, 2012, **51**, 4123.

23   K. H. Hopmann and A. Bayer, *Coord. Chem. Rev.*, 2014, **268**, 59.

24   E. Antolini, *ACS Catal.*, 2014, **4**, 1426.

25   J. M. Ketcham, I. Shin, T. P. Montgomery and M. J. Krische, *Angew. Chemie - Int. Ed.*, 2014, **53**, 9142.

26   D. M. Schultz and T. P. Yoon, *Science*, 2014, **343**, 1239176.

27   J. Xie, D.-H. Bao and Q.-L. Zhou, *Synthesis*, 2015, **47**, 460.

28   K. P. S. Zanoni, M. S. Sanematsu and N. Y. Murakami Iha, *Inorg. Chem. Commun.*, 2014, **43**, 162.

29   K. P. S. Zanoni, B. K. Kariyazaki, A. Ito, M. K. Brennaman, T. J. Meyer and N. Y. Murakami Iha, *Inorg. Chem.*, 2014, **53**, 4089.

30   L. Flamigni, A. Barbieri, C. Sabatini, B. Ventura and F. Barigelletti, *Top. Curr. Chem.*, 2007, **281**, 143.

31   T. Yutaka, S. Obara, S. Ogawa, K. Nozaki, N. Ikeda, T. Ohno, Y. Ishii, K. Sakai and M. Haga, *Inorg. Chem.*, 2005, **44**, 4737.

32   M. S. Lowry and S. Bernhard, *Chem. Eur. J.*, 2006, **12**, 7970.

33   J. A. G. Williams, A. J. Wilkinson and V. L. Whittle, *Dalton Trans.*, 2008, 2081.

34   Y. You and S. Y. Park, *Dalton Trans.*, 2009, 1267.

35   A. M. Prokhorov, A. Santoro, J. A. G. Williams and D. W. Bruce, *Angew. Chemie*, 2012, **51**, 95.

36   S. Sharma, H. Kim, Y. H. Lee, T. Kim, Y. S. Lee and M. H. Lee, *Inorg. Chem.*, 2014, **53**, 8672.

37   D. N. Chirdon, W. J. Transue, H. N. Kagalwala, A. Kaur, A. B. Maurer, T. Pintauer and S. Bernhard, *Inorg. Chem.*, 2014, **53**, 1487.

38   S. Takizawa, K. Shimada, Y. Sato and S. Murata, *Inorg. Chem.*, 2014, **53**, 2983.

39   F. Monti, A. Baschieri, I. Gualandi, J. J. Serrano-Pérez, J. M. Junquera-Hernández, D. Tonelli, A. Mazzanti, S. Muzzioli, S. Stagni, C. Roldan-Carmona, A. Pertegás, H. J. Bolink, E. Ortí, L. Sambri and N. Armaroli, *Inorg. Chem.*, 2014, **53**, 7709.

40   K. P. S. Zanoni, A. Ito and N. Y. Murakami Iha, *submitted*.

41   K. P. S. Zanoni, R. C. Amaral, B. K. Kariyazaki, R. L. Coppo and N. Y. Murakami Iha, Photophysical Elucidation of Emissive Ir(III) Complexes Towards Light-Emitting Devices (LEDs), in *XIII Brazilian MRS Meeting 2014 (João Pessoa, Brazil)*, 2014, 868.

42   A. W. Adamson, *J. Chem. Educ.*, 1983, **60**, 797.

43   G. B. Porter, *J. Chem. Educ.*, 1983, **60**, 785.

44   A. Ito and T. J. Meyer, *Phys. Chem. Chem. Phys.*, 2012, **14**, 13731.

45   A. R. G. Smith, P. L. Burn and B. J. Powell, *ChemPhysChem*, 2011, **12**, 2429.

46   M. Nonoyama, *Bull. Chem. Soc. Jpn.*, 1974, **47**, 767.

47   S. Lamansky, P. Djurovich, D. Murphy, F. Abdel-Razzaq, R. Kwong, I. Tsyba, M. Bortz, B. Mui, R. Bau and M. E. Thompson, *Inorg. Chem.*, 2001, **40**, 1704.

48   E. Baranoff, B. F. E. Curchod, F. Monti, F. Steimer, G. Accorsi, I. Tavernelli, U. Rothlisberger, R. Scopelliti, M. Grätzel and M. K. Nazeeruddin, *Inorg. Chem.*, 2012, **51**, 799.

49   F. Dumur, M. Lepeltier, H. Z. Siboni, D. Gigmes and H. Aziz, *Synth. Met.*, 2014, **198**, 131.

50   C. Shi, H. Sun, Q. Jiang, Q. Zhao, J. Wang, W. Huang and H. Yan, *Chem. Commun.*, 2013, **49**, 4746.

51   M. K. Nazeeruddin, R. Humphry-Baker, D. Berner, S. Rivier, L. Zuppiroli and M. Graetzel, *J. Am. Chem. Soc.*, 2003, **125**, 8790.

52   V. H. Nguyen, H. Q. Chew, B. Su and J. H. K. Yip, *Inorg. Chem.*, 2014, **53**, 9739.

53   A. Ionescu, E. I. Szerb, Y. J. Yadav, A. M. Talarico, M. Ghedini and N. Godbert, *Dalton Trans.*, 2014, **43**, 784.

54   K. Dedeian, P. I. Djurovich, F. O. Garces, G. Carlson and R. J. Watts, *Inorg. Chem.*, 1991, **30**, 1685.

55   J. Sun, W. Wu and J. Zhao, *Chem. Eur. J.*, 2012, **18**, 8100.

56   A. B. Tamayo, B. D. Alleyne, P. I. Djurovich, S. Lamansky, I. Tsyba, N. N. Ho, R. Bau and M. E. Thompson, *J. Am. Chem. Soc.*, 2003, **125**, 7377.

57   K. Dedeian, J. Shi, N. Shepherd, E. Forsythe and D. C. Morton, *Inorg. Chem.*, 2005, **44**, 4445.

58   A. R. McDonald, M. Lutz, L. S. Von Chrzanowski, G. P. M. Van Klink, A. L. Spek and G. Van Koten, *Inorg. Chem.*, 2008, **47**, 6681.

59   C. Dragonetti, L. Falciola, P. Mussini, S. Righetto, D. Roberto, R. Ugo, A. Valore, F. De Angelis, S. Fantacci, A. Sgamellotti, M. Ramon and M. Muccini, *Inorg. Chem.*, 2007, **46**, 8533.

60   H. J. Park, J. N. Kim, H. Yoo, K. Wee, S. O. Kang, D. W. Cho and U. C. Yoon, *J. Org. Chem.*, 2013, **78**, 8054.

61   S. Ladouceur, D. Fortin and E. Zysman-Colman, *Inorg. Chem.*, 2010, **49**, 5625.

62   F. De Angelis, S. Fantacci, N. Evans, C. Klein, S. M. Zakeeruddin, J.-E. Moser, K. Kalyanasundaram, H. J. Bolink, M. Gratzel and M. K. Nazeeruddin, *Inorg. Chem.*, 2007, **46**, 5989.

63   D.-L. Ma, V. P.-Y. Ma, D. S.-H. Chan, K.-H. Leung, H.-Z. He and C.-H. Leung, *Coord. Chem. Rev.*, 2012, **256**, 3087.

64   A. Endo, K. Suzuki, T. Yoshihara, S. Tobita, M. Yahiro and C. Adachi, *Chem. Phys. Lett.*, 2008, **460**, 155.

65   J. Zhuang, W. Li, W. Su, Y. Liu, Q. Shen, L. Liao and M. Zhou, *Org. Electron.*, 2013, **14**, 2596.

66   J. Frey, B. F. E. Curchod, R. Scopelliti, I. Tavernelli, U. Rothlisberger, M. K. Nazeeruddin and E. Baranoff, *Dalton Trans.*, 2014, **43**, 5667.

67   S. Fan, X. Zong, P. E. Shaw, X. Wang, Y. Geng, A. R. G. Smith, P. L. Burn, L. Wang and S.-C. Lo, *Phys. Chem. Chem. Phys.*, 2014, **16**, 21577.

68   Y. Li, N. Dandu, R. Liu, Z. Li, S. Kilina and W. Sun, *J. Phys. Chem. C*, 2014, **118**, 6372.

69   P. Li, G.-G. Shan, H.-T. Cao, D.-X. Zhu, Z.-M. Su, R. Jitchati and M. R. Bryce, *Eur. J. Inorg. Chem.*, 2014, **2014**, 2376.

70   Y. Chen, L. Qiao, L. Ji and H. Chao, *Biomaterials*, 2014, **35**, 2.

71   S. Lee, S.-O. Kim, H. Shin, H.-J. Yun, K. Yang, S.-K. Kwon, J.-J. Kim and Y.-H. Kim, *J. Am. Chem. Soc.*, 2013, **135**, 14321.

72   K. Hasan, L. Donato, Y. Shen, J. D. Slinker and E. Zysman-Colman, *Dalt. Trans.*, 2014, **43**, 13672.

73   S. Ladouceur, K. N. Swanick, S. Gallagher-Duval, Z. Ding and E. Zysman-Colman, *Eur. J. Inorg. Chem.*, 2013, **2013**, 5329.

74   J. Park, J. S. Park, Y. G. Park, J. Y. Lee, J. W. Kang, J. Liu, L. Dai and S.-H. Jin, *Org. Electron.*, 2013, **14**, 2114.

75   G.-N. Li, Y. Zou, Y.-D. Yang, J. Liang, F. Cui, T. Zheng, H. Xie and Z.-G. Niu, *J. Fluoresc.*, 2014, **24**, 1545.

76   R. Tao, J. Qiao, G. Zhang, L. Duan, L. Wang and Y. Qiu, *J. Phys. Chem. C*, 2012, **116**, 11658.

77   G. Zhang, H. Zhang, Y. Gao, R. Tao, L. Xin, J. Yi, F. Li, W. Liu and J. Qiao, *Organometallics*, 2014, **33**, 61.

78   P. Majumdar, X. Yuan, S. Li, B. Le Guennic, J. Ma, C. Zhang, D. Jacquemin and J. Zhao, *J. Mater. Chem. B*, 2014, **2**, 2838.

79   G. J. Barbante, E. H. Doeven, E. Kerr, T. U. Connell, P. S. Donnelly, J. M. White, T. Lópes, S. Laird, D. J. D. Wilson, P. J. Barnard, C. F. Hogan and P. S. Francis, *Chem. Eur. J.*, 2014, **20**, 3322.

80   T. Sajoto, P. I. Djurovich, A. B. Tamayo, J. Oxgaard, W. A. Goddard and M. E. Thompson, *J. Am. Chem. Soc.*, 2009, **131**, 9813.

81   M. Lepeltier, F. Dumur, B. Graff, P. Xiao, D. Gigmes, J. Lalevée and C. R. Mayer, *Helv. Chim. Acta*, 2014, **97**, 939.

82   C. Shi, H. Sun, X. Tang, W. Lv, H. Yan, Q. Zhao, J. Wang and W. Huang, *Angew. Chemie*, 2013, **52**, 13434.

83   A. M. Brouwer, *Pure Appl. Chem.*, 2011, **83**, 2213.

84   J. Li, P. I. Djurovich, B. D. Alleyne, M. Yousufuddin, N. N. Ho, J. C. Thomas, J. C. Peters, R. Bau and M. E. Thompson, *Inorg. Chem.*, 2005, **44**, 1713.

85   P. Chen and T. J. Meyer, *Inorg. Chem.*, 1996, **35**, 5520.

86   P. Chen and T. J. Meyer, *Chem. Rev.*, 1998, **98**, 1439.

87   A. S. Polo, M. K. Itokazu, K. M. Frin, A. O. T. Patrocínio and N. Y. Murakami Iha, *Coord. Chem. Rev.*, 2006, **250**, 1669.

88   D. Mochizuki, M. Sugiyama, M. M. Maitani and Y. Wada, *Eur. J. Inorg. Chem.*, 2013, **2013**, 2324.

89   M. K. Itokazu, A. S. Polo and N. Y. Murakami Iha, *J. Photochem. Photobiol. A Chem.*, 2003, **160**, 27.

90   A. S. Polo, M. K. Itokazu and N. Y. Murakami Iha, *J. Photochem. Photobiol. A Chem.*, 2006, **181**, 73.

91   C.-J. Chang, C.-H. Yang, K. Chen, Y. Chi, C.-F. Shu, M.-L. Ho, Y.-S. Yeh and P.-T. Chou, *Dalton Trans.*, 2007, **2007**, 1881.

92   H. Sun, L. Yang, H. Yang, S. Liu, W. Xu, X. Liu, Z. Tu, H. Su, Q. Zhao and W. Huang, *RSC Adv.*, 2013, **3**, 8766.

93   E. Baranoff and B. F. E. Curchod, *Dalton Trans.*, 2015, **44**, 8318.

94   G. F. Strouse, H. U. Güdel, V. Bertolasi and V. Ferretti, *Inorg. Chem.*, 1995, **34**, 5578.

95   Y. Komada, S. Yamauchi and N. Hirota, *J. Phys. Chem.*, 1986, **90**, 6425.

96   H. Yersin, A. F. Rausch, R. Czerwieniec, T. Hofbeck and T. Fischer, *Coord. Chem. Rev.*, 2011, **255**, 2622.

97　　M. G. Colombo and H. U. Güdel, *Inorg. Chem.*, 1993, **32**, 3081.

98　　M. G. Colombo, A. Hauser and H. U. Guedel, *Inorg. Chem.*, 1993, **32**, 3088.

99　　F. W. M. Vanhelmont, G. F. Strouse, H. U. Güdel, A. C. Stückl and H. W. Schmalle, *J. Phys. Chem.*, 1997, **101**, 2946.

100　F. W. M. Vanhelmont, H. U. Güdel, M. Förtsch and H.-B. Bürgi, *Inorg. Chem.*, 1997, **36**, 5512.

101　A. Tsuboyama, H. Iwawaki, M. Furugori, T. Mukaide, J. Kamatani, S. Igawa, T. Moriyama, S. Miura, T. Takiguchi, S. Okada, M. Hoshino and K. Ueno, *J. Am. Chem. Soc.*, 2003, **125**, 12971.

102　K. Dedeian, J. Shi, E. Forsythe, D. C. Morton and P. Y. Zavalij, *Inorg. Chem.*, 2007, **46**, 1603.

103　A. Ito, Y. Kang, S. Saito, E. Sakuda and N. Kitamura, *Inorg. Chem.*, 2012, **51**, 7722.

104　A. Ito, D. J. Stewart, T. E. Knight, Z. Fang, M. K. Brennaman and T. J. Meyer, *J. Phys. Chem. B*, 2013, **117**, 3428.

105　W. Wright, *Trans. Opt. Soc.*, 1929, **30**, 141.

106　T. Smith and J Guild, *Trans. Opt. Soc.*, 1931, **33**, 73.

107　CIE-Datatables: <http://www.cie.co.at/publ/abst/datatables15_2004/x2.txt> <http://www.cie.co.at/publ/abst/datatables15_2004/y2.txt> and http://www.cie.co.at/publ/abst/datatables15_2004/z2.txt>; accessed in November, 2014.

108　H. Round, *Electr. World*, 1907, 309.

109　O. Lossev, *Philos. Mag.*, 1928, **6**, 1024.

110　H. G. Grimmeiss and J. W. Allen, *J. Non-Cryst. Solids*, 2006, **352**, 871.

111　J. Allen and H. Grimmeiss, *Mater. Sci. Forum*, 2008, **590**, 1.

112   M. Novikov, *Phys. Solid State*, 2004, **46**, 1.

113   E. Schubert, *Light-Emitting Diodes*, Cambridge, New York, 2nd edn., 2003.

114   G. Destriau, *J. Chim. Phys.*, 1936, **33**, 587.

115   A. N. Krasnov, *Displays*, 2003, **24**, 73.

116   M. Bredol and H. S. Dieckhoff, *Materials*, 2010, **3**, 1353.

117   K. D. Jandt and R. W. Mills, *Dent. Mater.*, 2013, **29**, 605.

118   M. G. Craford, *Proc. IEEE*, 2013, **101**, 2170.

119   N. Holonyak and S. F. Bevacqua, *Appl. Phys. Lett.*, 1962, **1**, 82.

120   R. A. Logan, H. G. White and W. Wiegmann, *Appl. Phys. Lett.,* 1968, **13**, 139.

121   M. G. Craford, *J. Appl. Phys.*, 1972, **43**, 4075.

122   I. Akasaki, H. Amano, S. Sota, H. Sakai, T. Tanaka and M. Koike, *Jpn J. Appl. Physics,* 1995, **34**, L1517.

123   S. Nakamura, M. Senoh, S. Nagahama, N. Iwasa, T. Yamada, T. Matsushita, H. Kiyoku and Y. Sugimoto, *Jpn J. Appl. Phys.*, 1996, **35**, L74.

124   Class for Physics of the Royal Swedish Academy of Sciences, *Sci. Backgr. Nobel Prize Phys. 2014*, 2014, p1.

125   H. Kallman and M. Pope, *Nature*, 1960, **186**, 31.

126   M. Pope, H. P. Kallmann and P. Magnante, *J. Chem. Phys.*, 1963, **38**, 2042.

127   Y. Yang, *MRS Bull.*, 1997, 31.

128   J. K. Borchardt, *Mater. Today*, 2004, **7**, 42.

129   M. Baldo, S. Forrest and M. Thompson, Organic Phosphorescence, in *Organic Electroluminescence*, Taylor & Francis, Boca Raton, 2005, p267.

130   M. Baldo, D. O'Brien, Y. You, A. Shoustikov, S. Sibley, M. Thompson and S. Forrest, *Nature*, 1998, **395**, 151.

131   M. A. Baldo, S. Lamansky, P. E. Burrows, M. E. Thompson and S. R. Forrest, *Appl. Phys. Lett.*, 1999, **75**, 4.

132   T. Forster, *Discuss. Faraday Soc.*, 1959, **27**, 7.

133   D. L. Dexter, *J. Chem. Phys.*, 1953, **21**, 836.

134   M. Baldo, M. Thompson and S. Forrest, *Pure Appl. Chem.*, 1999, **71**, 2095.

135   K. P. S. Zanoni and N. Y. Murakami Iha, *work in progress.*

136   Q. Pei, G. Yu, C. Zhang, Y. Yang and A. J. Heeger, *Science*, 1995, **269**, 1086.

137   M. K. Nazeeruddin, R. T. Wegh, Z. Zhou, C. Klein, Q. Wang, F. De Angelis, S. Fantacci and M. Grätzel, *Inorg. Chem.*, 2006, **45**, 9245.

138   B. Minaev, H. Ågren and F. De Angelis, *Chem. Phys.*, 2009, **358**, 245.

139   J. Slinker, D. Bernards, P. L. Houston, H. D. Abruña, S. Bernhard and G. G. Malliaras, *Chem. Commun.*, 2003, **2003**, 2392.

140   H. Rudmann, S. Shimada and M. F. Rubner, *J. Appl. Phys.*, 2003, **94**, 115.

141   L. Schulz, L. Nuccio, M. Willis, P. Desai, P. Shakya, T. Kreouzis, V. K. Malik, C. Bernhard, F. L. Pratt, N. A. Morley, A. Suter, G. J. Nieuwenhuys, T. Prokscha, E. Morenzoni, W. P. Gillin and A. J. Drew, *Nat. Mater.*, 2011, **10**, 39.

142   J. D. Slinker, A. A. Gorodetsky, M. S. Lowry, J. Wang, S. Parker, R. Rohl, S. Bernhard and G. G. Malliaras, *J. Am. Chem. Soc.*, 2004, **126**, 2763.

143   J.-K. Lee, D. S. Yoo, E. S. Handy and M. F. Rubner, *Appl. Phys. Lett.*, 1996, **69**, 1686.

144   R. D. Costa, E. Ortí, H. J. Bolink, F. Monti, G. Accorsi and N. Armaroli, *Angew. Chem. Int. Ed.*, 2012, **51**, 8178.

145   R. D. Costa, E. Ortí, H. J. Bolink, S. Graber, S. Schaffner, M. Neuburger, C. E. Housecroft and E. C. Constable, *Adv. Funct. Mater.*, 2009, **19**, 3456.